Regulating Lipid Composition Rationalizes Acyl Tail Saturation Homeostasis in Ectotherms

Girard, M.; Bereau, T.

DOI
10.1016/j.bpj.2020.07.024

Publication date
2020

Document Version
Final published version

Published in
Biophysical Journal

Biophysical Journal
Article

Biophysical Society

Regulating Lipid Composition Rationalizes Acyl Tail Saturation Homeostasis in Ectotherms

Martin Girard[1,*] and Tristan Bereau[1,2]
[1]Max Planck Institute for Polymer Research, Mainz, Germany and [2]Van 't Hoff Institute for Molecular Sciences and Informatics Institute, University of Amsterdam, Amsterdam, the Netherlands

ABSTRACT Cell membranes mainly consist of lipid bilayers with an actively regulated composition. The underlying processes are still poorly understood, in particular, how the hundreds of components are controlled. Cholesterol has been found to correlate with phospholipid saturation for reasons that remain unclear. To better understand the link between cell membrane regulation and chemical composition, we establish a computational framework based on chemical reaction networks, resulting in multiple semigrand canonical ensembles. By running computer simulations, we show that regulating the chemical potential of lipid species is sufficient to reproduce the experimentally observed increase in acyl tail saturation with added cholesterol. Our model proposes a different picture of lipid regulation in which components can be regulated passively instead of actively. In this picture, phospholipid acyl tail composition naturally adapts to added molecules such as cholesterol or proteins. A comparison between regulated membranes with commonly studied ternary model membranes shows stark differences: for instance, correlation lengths and viscosities observed are independent of lipid chemical affinity.

SIGNIFICANCE We run computer simulations of a lipid bilayer. Instead of fixing its composition, we passively regulate it via semigrand canonical ensembles. Our simple model reproduces correlations observed in vivo between cholesterol content and saturation levels of phospholipid acyl tails. Membrane properties such as viscosity are largely independent of phospholipid composition, suggesting a decoupling from lipid composition in complex membranes.

INTRODUCTION

For eukaryotes, the plasma membrane is the last interface between the cell interior and the extracellular environment. It is responsible for regulating permeation of molecules (1,2), and membrane protein function (3,4). Cell membranes mainly consist of lipid bilayers. In aqueous environments, the amphiphilic molecules forming these structures, which are comprised of a polar headgroup and hydrocarbon tails, readily self-assemble to hydrate the polar head while minimizing hydrophobic interactions of apolar tails. Phospholipids can be broadly classified by their headgroup (phosphatidylcholine, phosphatidylserine, etc.). Most phospholipids in biological membranes have two hydrocarbon tails, and their nature is generally widely variable, ranging from 12 to 24 carbons with varying degrees of saturation. When considering both classifications, this yields hundreds to thousands of different lipid types (5). Furthermore, biological membranes are generally asymmetric: the two leaflets of the bilayers have different compositions, which is maintained by transmembrane proteins pumping specific lipids from one leaflet to the other (6). Similar complexity is replicated by various lipid membranes inside the cell and, although advances have been made by lipidomics, many fundamental questions still need to be answered (7).

Membrane regulation is one of the most poorly understood areas of biological membrane physics. The question of how and why various properties are regulated is of great interest to biology. For instance, there are differences in composition of various membranes within single cells that are thought to endow the membrane with specific properties (8). Lipid tail composition is often thought to be regulated by specific pathways activated by sensor proteins in the membrane, but little is known about them (9). Based on experimental observations, two physical properties are perceived as tightly regulated in plasma membranes: viscosity (10,11) and curvature (12), which correlate in vivo (13). Regulation of viscosity includes acyl tail remodeling via the Lands cycle (14–16), a process through which lipids change

Submitted December 9, 2019, and accepted for publication July 6, 2020.
*Correspondence: martin.girard@mpip-mainz.mpg.de
Editor: Markus Deserno.
https://doi.org/10.1016/j.bpj.2020.07.024

the nature of their acyl tails. Membrane curvature regulation involves multiple factors. Some of them are internal to membrane chemistry, for instance phosphatidylethanolamine carries a small headgroup, which gives the lipid a conical shape and can induce curvature (17). However, it may also involve external factors to the membrane, such as action of the cytoskeleton (18). Another quantity has recently emerged as being regulated in cells: the difference between ambient and bilayer demixing temperature (T_m). Whether T_m is regulated through the same mechanism as viscosity or simply as a byproduct of its regulation is currently unknown. Additionally, although there is a clear link between T_m and proximity to the critical temperature needed for lipid rafts, the picture remains incomplete. However, experiments presented in (19) clearly demonstrate that lowering the incubation temperature of zebrafish cells by $\sim$12 K lowers T_m of their plasma membranes by $\sim$12 K, an astounding precision considering how much the membrane composition changes in the process.

Cholesterol appears to play an important role in cell homeostasis but, here again, the exact mechanisms are not fully understood. Its concentration in cell membranes is tightly regulated (20–23) and strongly affects membrane properties. It reduces diffusion (24) and raises nematic order in liquid phases (25,26). It is known to be involved in raft formation (27,28) and registration (29) by preferentially partitioning in ordered phases, rich in high-T_m saturated phospholipids (28,30). Cholesterol levels in membranes also appear correlated with phospholipid saturation contents (9,10,19), leading to different phenomena: an increase in cholesterol in model membranes of purified components and in cells will lead to a decrease (31) and increase (19) of T_m, respectively.

To rationalize some of these findings using computer simulations, the composition must be allowed to fluctuate. This is elegantly achieved by controlling the chemical potential—the thermodynamic variable conjugate to composition. Alternatively, differences between chemical potentials of different chemical species can be fixed, yielding the semigrand canonical (SGC) ensemble. This keeps the overall number of molecules fixed, a more suitable approach for molecular dynamics, as compared to the grand canonical ensemble. Furthermore, chemical reaction networks, sets of reactants, products and reactions, can be expressed into chemical potential differences (32) between molecules and large-scale, parallel algorithms have been developed for this ensemble (33).

Here, we introduce the regulated thermodynamic ensemble (RTE), a collection of SGC ensembles to emulate regulation pathways in cells. This enables us to model complex membrane biochemistry and gain insight into biological implications. We apply this methodology to a phosphatidylcholine (PC) membrane incorporating various amounts of cholesterol. We show that regulating the chemical potential of lipid species is sufficient to reproduce the experimentally observed increase in acyl tail saturation with added cholesterol (9,10,19). Beyond the overall trend, our distributions of saturations are in line with lipidomics studies (19): phospholipids that contain zero or one unsaturation increase with cholesterol, whereas others decrease.

METHODS

In this section, we introduce a hypothetical regulation pathway to illustrate the collection of SGC ensembles. We make a connection with the biological pathway responsible for remodeling the acyl tail nature, although similar arguments can be applied to other mechanisms involving chemical networks (9). The RTE can be used to describe out-of-equilibrium systems, such as asymmetric membranes, and derived results should be associated with homeostasis or stationary states rather than a thermodynamic equilibrium in the usual sense because chemical potential differences can be enforced.

Let us consider a simple lipid bilayer, with only two classes of lipids (headgroups) and acyl tails of varying saturation, as illustrated in Fig. 1 *A*. Inside the cell, lipid transport proteins (LTP) provide most of the trafficking and we neglect vesicular transport (34) for simplicity. LTPs transport lipids from one membrane to another, and we hypothesize that regulatory transport mainly takes place with the endoplasmic reticulum (ER). For simplicity, we also discard effects of other proteins present in biological membranes (35).

In this picture, lipids present on the plasma membranes are simply a subset of a wider chemical reaction network, which includes remodeling in ER and transport by LTP. The former implies formation of a protein-lipid complex, which involves at least partial extraction of the lipid, creating a free energy barrier to form the complex. For a lipid of species s in a membrane with a given composition, rates of formation of complexes depend on the free energy difference of the lipid between barrier and membrane states. Once a lipid molecule is remodeled, membrane composition changes, the free energy decreases, and remodeling becomes slower. If the system is at equilibrium and closed, then it converges toward the global free energy minimum. At this point, the gradient of the free energy with respect to composition—corresponding to the chemical potential μ—is zero, and so is the chemical potential difference between any two lipid species s and s' ($\Delta\mu_{s,\,s'} = 0$). Enzymatic pathways are usually described by complex kinetics (32,36,37) that can drive the system away from equilibrium. Nevertheless, we will approximate the bilayer at equilibrium ($\Delta\mu_{s,\,s'} = 0$), which we call the equal-binding approximation. Below, we detail the chemical processes in the ER, what the equal-binding approximation entails, and how it could later be refined.

The Lands cycle, the acyl tail remodeling process, is an interesting chemical network because it involves many lipid species, but few enzymes. These are able to cleave an acyl tail from a PC molecule, yielding a fatty acid and a lysophosphatidylcholine (LPC) or to attach a coenzyme A-fatty acid complex onto an LPC molecule to produce a PC (14,15,38,39). External cofactors such as ATP can enforce a chemical potential difference between all PC and LPC species ($\Delta\mu_{s,\,s'} \neq 0$), which is dependent on cofactor concentrations and affinities (i.e., binding rates to different substrates). If multiple chemical networks are isolated as a function of external cofactors, then each network constitutes a single SGC ensemble.

Within the equal-binding approximation, we implement a few assumptions to make our calculations tractable: 1) acetylation is fast, such that LPC are only involved as reaction intermediates; 2) phospholipases do not selectively hydrolyze lipids; and 3) a molecule that experiences the Lands cycle—hydrolyzed and acetylated—simply swaps one of its tails according to a distribution at chemical equilibrium. As a result, we neglect the selectivity of acyltransferase proteins. In addition, our regulation of fatty acids is done implicitly. If all these conditions are satisfied, all phospholipids are at equilibrium with $\Delta\mu_{s,s'} = 0$.

This set of approximations offers a simple conceptual framework to regulate lipids but naturally conveys caveats. The first approximation seems reasonable because LPC, and lysophospholipids in general, are minor component of membranes. However, the two other approximations are

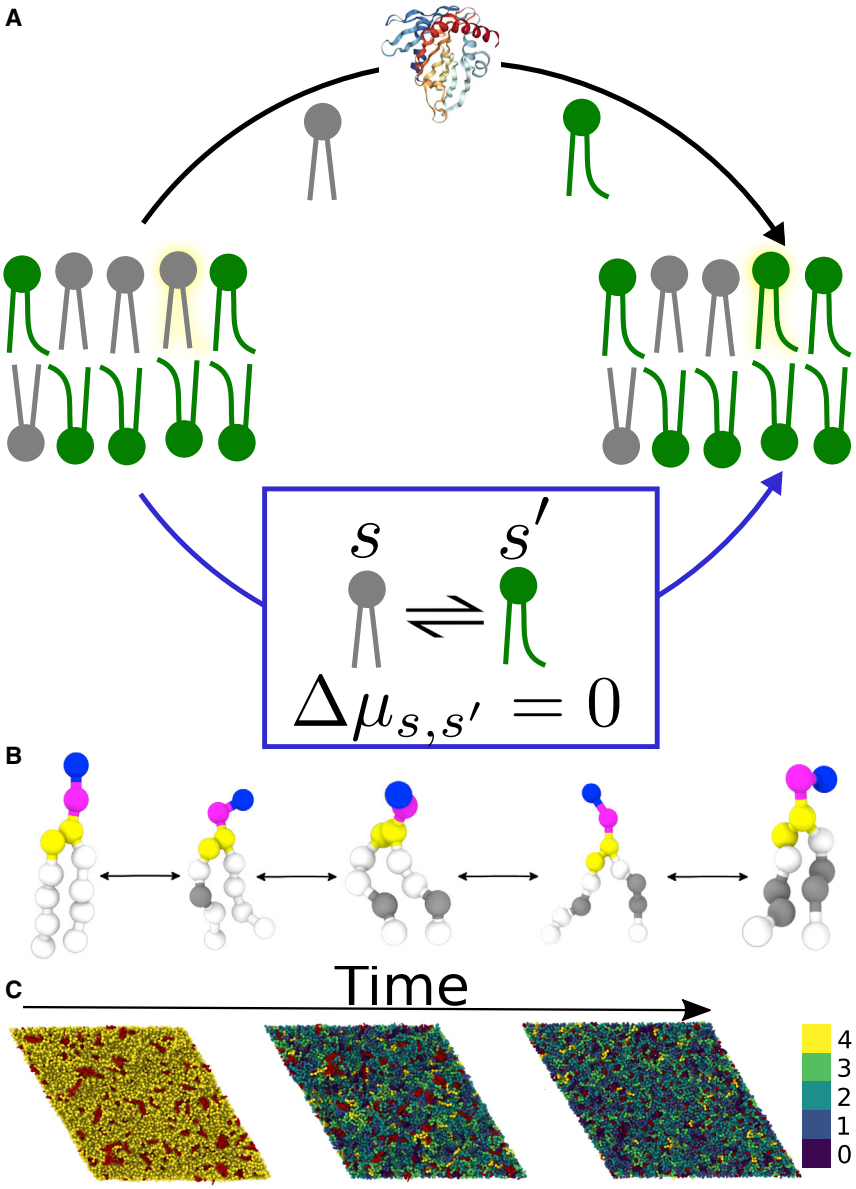

FIGURE 1 (*A*) Sketch of the regulatory processes used for our argument. Lipids are moved from the ER to other membranes through LTP, which carry over chemical potential differences (phosphatidylcholine transport protein PDB: 1LN1 depicted here). Lipids being able to transform from one to another through the Lands cycle, indicated by arrows, belong to a single SGC, depicted here by rectangles. The remodeling cycle enforces chemical potential differences within the SGC ensemble, which is then carried to other membranes by LTP. Headgroup composition is fixed as head groups are not able to remodel from one to another. (*B*) Representative ensemble of PC molecules used in molecular dynamics, with different degrees of unsaturation. During simulation, at each Monte Carlo event, molecules may gain or lose an unsaturated bond. Unsaturations are located on gray beads and only the two middle beads of each chain can be unsaturated. Because there are multiple locations available for unsaturation, many different molecules may have the same degree of unsaturation. (*C*) Time evolution of a lipid bilayer initialized with two unsaturations per acyl tail. The left side shows initial relaxation and thermalization (after 1 ns), the middle shows after 100 ns, and the right side shows after 15 μs. In highly unsaturated membranes, cholesterol tends to form aggregates which dissolve upon chemical relaxation. Numerically, composition relaxation is faster than cholesterol diffusion and dispersion throughout the layer. Lipids are colored by unsaturations, ranging from zero (*blue*) to four (*yellow*), whereas cholesterol is colored red. To see this figure in color, go online.

more stringent because proteins involved in the Lands cycle are known to be highly selective. In particular, unsaturated acyl chains are preferentially located on glycol position *sn2* (16). Furthermore, the regulation of fatty acids operate quite differently from the Lands cycle because biology does not go by the equal-binding approximation and tends to suit particular biological needs (40). However, we can still infer general trends in the mechanism, with the caveat that membrane composition of a particular species will be more complex than our model. We therefore expect the population distributions to be shifted from actual plasma membranes. A potential extension would be to incorporate the underlying chemical reaction network in an ER simulation and extracting the relevant chemical potential differences. However, it is presently outside the scope of this article.

RESULTS AND DISCUSSION

Making use of the equal-binding approximation, we consider a simple RTE lipid membrane consisting of a single SGC ensemble, constituted by 16:(0–2), 16:(0–2) PC molecules (with 0–2 unsaturations per acyl tail; see Fig. 1, *B* and *C* and Supporting Material for a full list), and mixed with cholesterol. Overall, the PC SGC ensemble contains 16 distinct lipid molecules. We consider a mixture of 1600 PC molecules along with a molar fraction of 10–30% cholesterol. Systems are kept at constant temperature between 289 and 314 K ($k_BT = 2.4 - 2.6$ kJ/mol) and use a variant of the MARTINI force field (see Supporting Material).

Additionally, to mitigate potential force field effects, we tested different levels of interactions in our force field (see Supporting Material for details). Effectively, our modifications tune the affinity between saturated and unsaturated portions of the acyl tails, similar to the χ-parameter of solution models. This parameter measures the relative strength

of like versus unlike interactions, having a low value if unlike molecules prefer to aggregate, thus driving mixing, and a high value if like molecules prefer each other, which drives segregation. We therefore label high chemical affinity by "low-χ" and low chemical affinity by "high-χ." All systems show a single homogeneous phase, as shown in Fig. 1 *C*. Furthermore, we have simulated an unregulated system with a phospholipid composition taken from the low-χ-regulated ensemble at 14% cholesterol, labeled "No Reg."

Unlike usual fixed composition model membranes, the composition dynamically changes with cholesterol fraction. The lipid-unsaturation fraction—the fraction of lipids in the membrane with a given number of unsaturations—is shown in Fig. 2, *A* and *B* for the low and high χ-models. The trends qualitatively match those observed in zebrafish (19), that is lipids with zero or one unsaturation increase with cholesterol, whereas others decrease (see Fig. 2, *A* and *B*). The behavior is independent of the MARTINI model used, suggesting that the mechanism is general for liquid phases. Cholesterol appears as a saturating agent in these membranes, i.e., the proportion of acyl chains with low unsaturation increases with cholesterol. This is associated with a decrease in area per lipid in the membrane (see Fig. S1), meaning that an increase in cholesterol increases packing. Because saturated lipids pack better, their proportion increases, and this explains the bias toward saturated tails as cholesterol is added. As a general rule, unsaturations positioned far from the headgroup are preferred by cholesterol. A weak preference for unsaturations to be located on glycol carbon position *sn*1 over *sn*2 is also observed in our simulations, a phenomenon that does not happen in biological systems because of protein selectivity when phospholipids are formed: *sn*1 is preferentially saturated (16).

In the low χ-regime, populations of individual species are similar, leading to the lipid-unsaturation fraction being shaped by the binomial distribution of molecule types

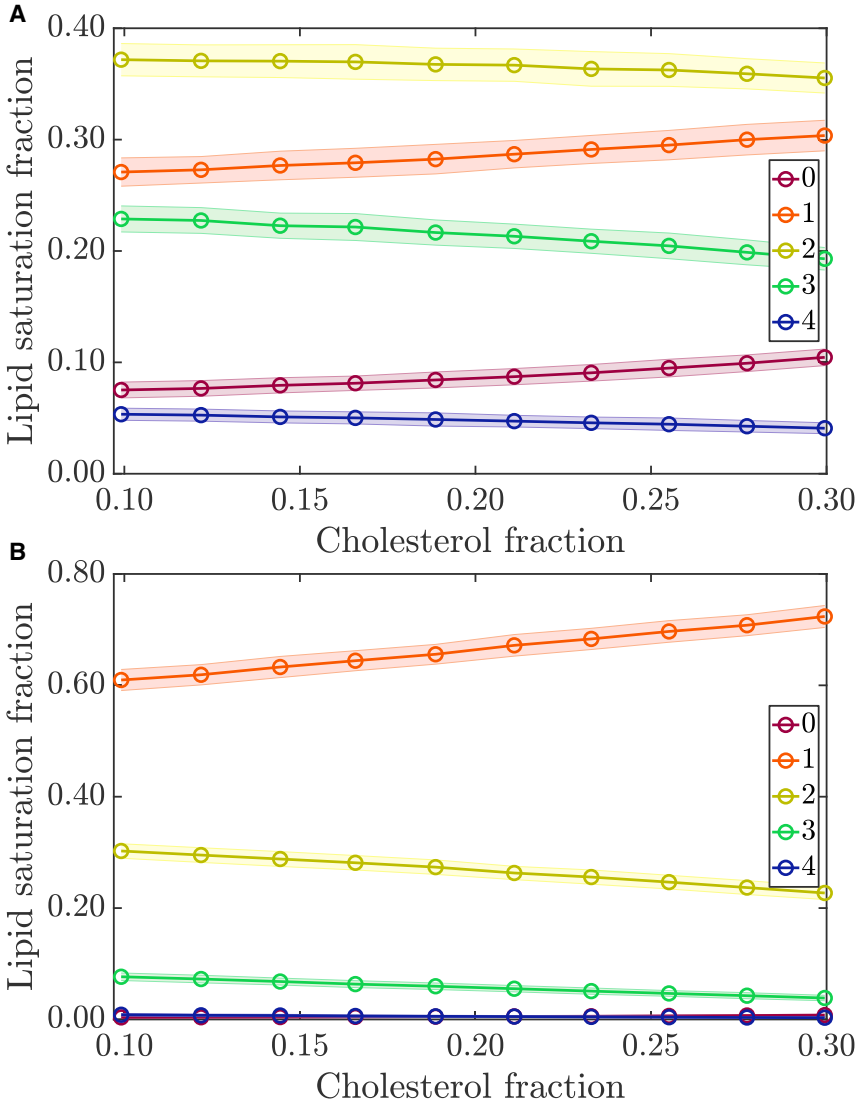

FIGURE 2 (*A*) and (*B*), lipid tail composition of 16:(0–2), 16:(0–2) PC lipids under the equal-binding approximation at $k_BT = 2.5$ for (*A*) low χ-parameter and (*B*) high χ-parameter. Color indicates the overall number of unsaturations on the lipid molecule. Note the different axis scales for (*A*) and (*B*). Shaded area indicates the standard deviation of the data. To see this figure in color, go online.

(Fig. 2 *A*). We conclude that the regime is dominated by the entropy of mixing. On the other hand, the high χ-model impairs significant differences in interactions between saturated and unsaturated groups and we predominantly observe single unsaturations. We conclude that this regime is dominated by enthalpic interactions. Changes in composition are also significantly larger in this regime (see Fig. 3). For low χ-lipids, increasing temperature tends to decrease saturation (see Fig. S3). Moreover, it lowers the response of the membrane to changes in cholesterol concentration, for both viscosity and composition. This arises from the mixing entropy, which has a contribution to the free energy proportional to temperature and tends toward equal lipid species concentrations. In biological membranes, fatty acids located on *sn*1 are mostly saturated and the few exceptions involve unsaturated fatty acids on *sn*2 (41). This may be a way to counteract dominance of the mixing free energy as it strongly reduces the available number of polyunsaturated species.

Lipid composition aside, our results reproduce well-established trends of cholesterol in lipid membranes. The nematic order parameter, characterized by the largest eigenvalue of the de Gennes Q-tensor, λ_+, is characteristic of liquid-disordered phases and increases with cholesterol fraction (see Fig. 4), a known effect in fluid membranes (42). Increases in temperature also cause the nematic order to decrease. When the cholesterol concentration is increased from 10 to 30%, the lateral diffusion constant reduces by a factor 2–3 (see Fig. S2), whereas the viscosity increases by a similar amount (factor of 3–4, see Fig. 4 *C*). Although the values of viscosity observed here ($\sim 10^{-2}$–10^{-1} P) are much lower than previously reported values in (11), they are in line with other simulations of lipid bilayers (43,44). The change in diffusion with cholesterol was previously reported in biological-like membranes (24) and thus suggests lipid packing as the main determinant of diffusion. Characterizing the correlation of the nematic order parameter in the RTE shows short correlation lengths (Fig. 4 *B*), which increase with cholesterol and decrease with temperature, similar to λ_+. Correlation length diverge when approaching critical demixing points and these results suggest that T_m increases with cholesterol concentration, but that T_m is too low to be accessible in our simulations. Similar behavior is observed for λ_+, correlation lengths and viscosity, which has implications when attempting to understand biological behavior from model ternary membranes.

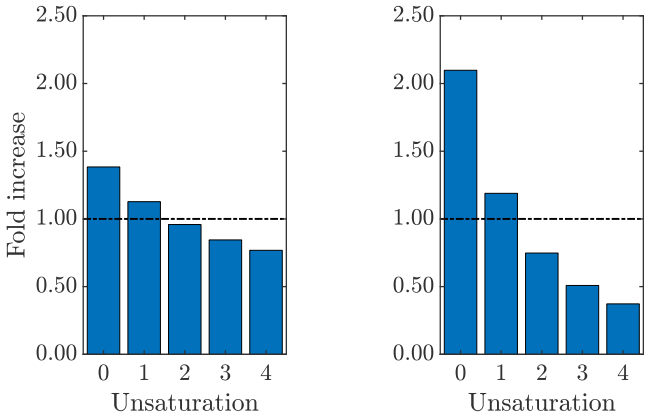

FIGURE 3 Compositions changes viewed as fold increase of the unsaturation contents of the membrane between 30 and 10% cholesterol. (*left*) Low-χ-membrane and (*right*) high-χ-membrane are shown. To see this figure in color, go online.

Although the membrane composition (Fig. 2) can change quite drastically with cholesterol and with variations of the MARTINI force field, properties shown in Fig. 4 are remarkably similar. The associated trends remain similar in the absence of regulation, so long as its fixed composition was taken from a regulated simulation ("No Reg"). However, behavior of our complex membranes appears very different than usual ternary model membranes. In our complex membranes, only cholesterol content and temperature affect viscosity, whereas, in ternary mixtures, phospholipid saturation also strongly affects dynamical properties such as viscosity, and this has been the rationale to explain changes in saturation contents of cells (10,45). This suggests that lipid saturation contents in eukaryote membranes does not play the same role as in model ternary membranes and may explain the shortcomings of simple models of biological membranes (40).

CONCLUSIONS

The regulated ensembles presented in this article shine a new light on acyl tail regulation: an accurate modeling of lipid saturation can be obtained simply as a consequence of the other components, such as cholesterol, and need not be actively regulated. It suffices to qualitatively reproduce cholesterol trends observed in zebrafish (19), in which an increase in cholesterol causes a decrease of acyl tail saturation as well as increased viscosity and correlation lengths of the membrane. Such a passive regulation scheme highlights the essential role of cholesterol to control both viscosity and T_m. In fact, our results closely resemble experimental observations in zebrafish (19), in which lipids with no tail or only one saturated tail become more prevalent at higher temperatures, along with cholesterol concentration. It is also reminiscent of trends observed along the secretory pathway, in which cholesterol concentration increases (9) along with acyl tail saturation (10). Properties of complex membrane studied here also differ from usual ternary mixtures. The saturation content has little effect on viscosity, suggesting that some properties tied to composition in model membranes, are decoupled from composition in complex membranes.

This framework offers many opportunities to further improve the description of complex biological cellular processes. Many biological phenomena naturally arise from the model, notably correlations between cholesterol

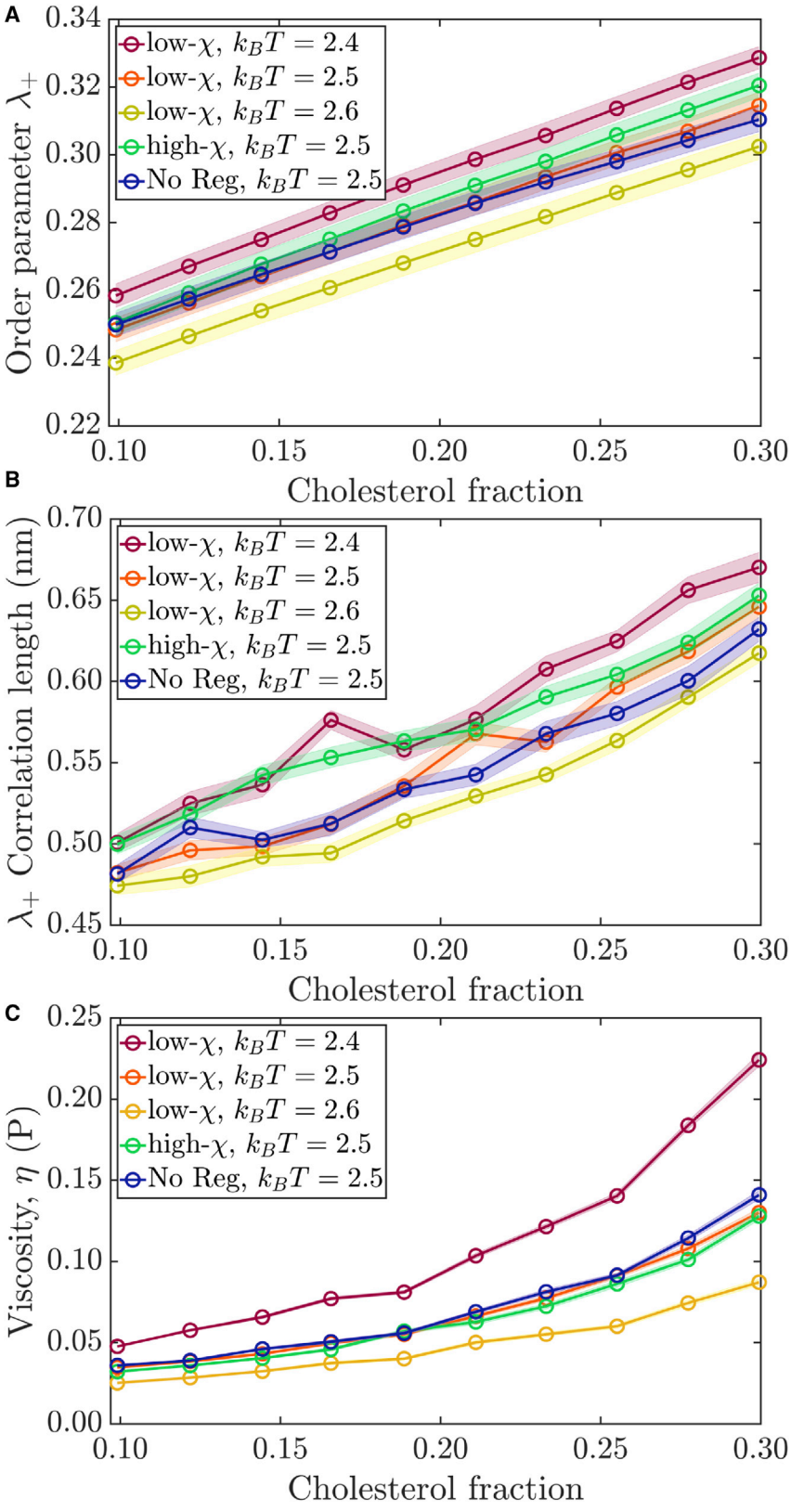

FIGURE 4 Complex membrane properties show weak dependence on phospholipid composition. The "No Reg" simulation corresponds to a fixed phospholipid composition taken from a regulated simulation from the low$-\chi$ force field with 14% cholesterol and $k_BT = 2.5$. (*A*) Nematic order of lipid molecules in the system is shown. (*B*) Correlation length of the nematic order parameter is shown. (*C*) Viscosity of the membrane as a function of cholesterol fraction is shown. Shaded area indicates the standard deviation of the data or the confidence interval of the fitting procedure. Temperature is expressed in kJ/mol. To see this figure in color, go online.

and phospholipid saturation. In principle, membrane composition will further be affected by additives, thereby affecting various properties (e.g., correlation length). Absent of the current model are proteins, which constitute a large portion of the surface of biological membranes, and likely influence T_m. Some of these are known to bind preferentially to specific lipids (35,46,47) and induce domain formation, whereas others bind to the actin network, which is hypothesized to be involved in membrane structure regulation (48–50). Nevertheless, the RTE predicts that passive regulation will cause membranes to specialize even without external input: cells that incorporate different proteins should naturally lead to different compositions. It could also be used to model cell response to membrane insertion of various compounds, such as drugs and anesthetics.

The equal-binding approximation, whereas a more faithful description than usual ternary model membranes, could be improved to better account for the relevant biology. More work is needed to better approximate the chemical networks involved, in particular to understand which ones can be easily extracted into SGCs and how to better approximate chemical potential differences between lipid species to lift the equal-binding approximation. Although there is considerable overlap between lipids chosen here and those found in biological membranes, there are discrepancies between the two sets. Notably, our lipids allow too many unsaturations on *sn*1 and only a single acyl chain length on *sn*2. Better lipid sets, closer available lipids in cells, will be tackled in future research, along with the modeling of asymmetric membranes. In the mean time, we hope that further experiments can lead to more insights into a chemical-network-based regulation mechanism and provide concrete evidence into the RTE.

Software

Simulations were run in the HOOMD-blue molecular dynamics engine (51, 52). Systems were assembled using the hoobas molecular builder (53). Simulations are run using a slight modification to the MARTINI force-field (54) (see Supporting Material). Visualization was done using the Ovito package (55). Data analysis was done using custom C++ code on top of publicly available C gsd API.

SUPPORTING MATERIAL

Supporting Material can be found online at https://doi.org/10.1016/j.bpj.2020.07.024.

AUTHOR CONTRIBUTIONS

M.G. and T.B. designed the research. M.G. carried out all simulations and analyzed the data. M.G. and T.B. wrote the article.

ACKNOWLEDGMENTS

We acknowledge Bernadette Mohr, Joseph F. Rudzinski, and Alessia Centi for critical review of this manuscript and Burkhard Dünweg for insightful discussions.

This project was supported by the Deutsche Forschungsgemeinschaft and the Alexander von Humboldt-Stiftung. This work used computational resources from the Max Planck Computing and Data Facility.

REFERENCES

1. Shinoda, W. 2016. Permeability across lipid membranes. *Biochim. Biophys. Acta.* 1858:2254–2265.
2. Yang, N. J., and M. J. Hinner. 2015. Getting across the cell membrane: an overview for small molecules, peptides, and proteins. *In* Site-Specific Protein Labeling: Methods and Protocols. Methods in Molecular Biology. A. Gautier and M. J. Hinner, eds. Springer, pp. 29–53.
3. Brown, M. F. 1994. Modulation of rhodopsin function by properties of the membrane bilayer. *Chem. Phys. Lipids.* 73:159–180.
4. Brown, M. F. 2017. Soft matter in lipid-protein interactions. *Annu. Rev. Biophys.* 46:379–410.
5. Sud, M., E. Fahy, …, S. Subramaniam. 2007. LMSD: LIPID MAPS structure database. *Nucleic Acids Res.* 35:D527–D532.
6. Daleke, D. L. 2003. Regulation of transbilayer plasma membrane phospholipid asymmetry. *J. Lipid Res.* 44:233–242.
7. Harayama, T., and H. Riezman. 2018. Understanding the diversity of membrane lipid composition. *Nat. Rev. Mol. Cell Biol.* 19:281–296.
8. Barelli, H., and B. Antonny. 2016. Lipid unsaturation and organelle dynamics. *Curr. Opin. Cell Biol.* 41:25–32.
9. Holthuis, J. C. M., and A. K. Menon. 2014. Lipid landscapes and pipelines in membrane homeostasis. *Nature.* 510:48–57.
10. Ernst, R., C. S. Ejsing, and B. Antonny. 2016. Homeoviscous adaptation and the regulation of membrane lipids. *J. Mol. Biol.* 428:4776–4791.
11. Sinensky, M. 1974. Homeoviscous adaptation–a homeostatic process that regulates the viscosity of membrane lipids in *Escherichia coli*. *Proc. Natl. Acad. Sci. USA.* 71:522–525.
12. Gruner, S. M. 1985. Intrinsic curvature hypothesis for biomembrane lipid composition: a role for nonbilayer lipids. *Proc. Natl. Acad. Sci. USA.* 82:3665–3669.
13. Dymond, M. K. 2016. Mammalian phospholipid homeostasis: evidence that membrane curvature elastic stress drives homeoviscous adaptation in vivo. *J. R. Soc. Interface.* 13:20160228.
14. Lands, W. E. 1960. Metabolism of glycerolipids. 2. The enzymatic acylation of lysolecithin. *J. Biol. Chem.* 235:2233–2237.
15. Lands, W. E., and I. Merkl. 1963. Metabolism of glycerolipids. III. Reactivity of various acyl esters of coenzyme A with alpha'-acylglycerophosphorylcholine, and positional specificities in lecithin synthesis. *J. Biol. Chem.* 238:898–904.
16. Shindou, H., and T. Shimizu. 2009. Acyl-CoA:lysophospholipid acyltransferases. *J. Biol. Chem.* 284:1–5.
17. McMahon, H. T., and E. Boucrot. 2015. Membrane curvature at a glance. *J. Cell Sci.* 128:1065–1070.
18. Jarsch, I. K., F. Daste, and J. L. Gallop. 2016. Membrane curvature in cell biology: an integration of molecular mechanisms. *J. Cell Biol.* 214:375–387.
19. Burns, M., K. Wisser, …, S. L. Veatch. 2017. Miscibility transition temperature scales with growth temperature in a zebrafish cell line. *Biophys. J.* 113:1212–1222.
20. Steck, T. L., and Y. Lange. 2010. Cell cholesterol homeostasis: mediation by active cholesterol. *Trends Cell Biol.* 20:680–687.
21. Ikonen, E. 2008. Cellular cholesterol trafficking and compartmentalization. *Nat. Rev. Mol. Cell Biol.* 9:125–138.

22. Chang, T.-Y., C. C. Y. Chang, …, Y. Yamauchi. 2006. Cholesterol sensing, trafficking, and esterification. *Annu. Rev. Cell Dev. Biol.* 22:129–157.
23. Goldstein, J. L., R. A. DeBose-Boyd, and M. S. Brown. 2006. Protein sensors for membrane sterols. *Cell.* 124:35–46.
24. Sharma, S., B. N. Kim, …, M. Lindau. 2015. A coarse grained model for a lipid membrane with physiological composition and leaflet asymmetry. *PLoS One.* 10:e0144814.
25. Daily, M. D., B. N. Olsen, …, N. A. Baker. 2014. Improved coarse-grained modeling of cholesterol-containing lipid bilayers. *J. Chem. Theory Comput.* 10:2137–2150.
26. Ferreira, T. M., F. Coreta-Gomes, …, D. Topgaard. 2013. Cholesterol and POPC segmental order parameters in lipid membranes: solid state 1H-13C NMR and MD simulation studies. *Phys. Chem. Chem. Phys.* 15:1976–1989.
27. Schmid, F. 2017. Physical mechanisms of micro- and nanodomain formation in multicomponent lipid membranes. *Biochim. Biophys. Acta Biomembr.* 1859:509–528.
28. Silvius, J. R. 2003. Role of cholesterol in lipid raft formation: lessons from lipid model systems. *Biochim. Biophys. Acta.* 1610:174–183.
29. Pantelopulos, G. A., and J. E. Straub. 2018. Regimes of complex lipid bilayer phases induced by cholesterol concentration in MD simulation. *Biophys. J.* 115:2167–2178.
30. Ge, M., K. A. Field, …, J. H. Freed. 1999. Electron spin resonance characterization of liquid ordered phase of detergent-resistant membranes from RBL-2H3 cells. *Biophys. J.* 77:925–933.
31. Veatch, S. L., and S. L. Keller. 2005. Seeing spots: complex phase behavior in simple membranes. *Biochim. Biophys. Acta.* 1746:172–185.
32. Rao, R., and M. Esposito. 2016. Nonequilibrium thermodynamics of chemical reaction networks: wisdom from stochastic thermodynamics. *Phys. Rev. X.* 6:041064.
33. Sadigh, B., P. Erhart, …, L. Zepeda-Ruiz. 2012. Scalable parallel Monte Carlo algorithm for atomistic simulations of precipitation in alloys. *Phys. Rev. B.* 85:184203.
34. Wong, L. H., A. T. Gatta, and T. P. Levine. 2019. Lipid transfer proteins: the lipid commute via shuttles, bridges and tubes. *Nat. Rev. Mol. Cell Biol.* 20:85–101.
35. Corradi, V., E. Mendez-Villuendas, …, D. P. Tieleman. 2018. Lipid-protein interactions are unique fingerprints for membrane proteins. *ACS Cent. Sci.* 4:709–717.
36. Michaelis, L., and M. L. Menten. 1913. Die Kinetik der Invertinwirkung. *Biochem. Z.* 49:333–369.
37. Beard, D. A., S. D. Liang, and H. Qian. 2002. Energy balance for analysis of complex metabolic networks. *Biophys. J.* 83:79–86.
38. Merkl, I., and W. E. Lands. 1963. Metabolism of glycerolipids. IV. Synthesis of phosphatidylethanolamine. *J. Biol. Chem.* 238:905–906.
39. MacDonald, J. I., and H. Sprecher. 1991. Phospholipid fatty acid remodeling in mammalian cells. *Biochim. Biophys. Acta.* 1084:105–121.
40. Bernardino de la Serna, J., G. J. Schütz, …, M. Cebecauer. 2016. There is no simple model of the plasma membrane organization. *Front. Cell Dev. Biol.* 4:106.
41. Yamashita, A., Y. Hayashi, …, T. Sugiura. 2014. Acyltransferases and transacylases that determine the fatty acid composition of glycerolipids and the metabolism of bioactive lipid mediators in mammalian cells and model organisms. *Prog. Lipid Res.* 53:18–81.
42. Wang, Y., P. Gkeka, …, Z. Cournia. 2016. DPPC-cholesterol phase diagram using coarse-grained Molecular Dynamics simulations. *Biochim. Biophys. Acta.* 1858:2846–2857.
43. Venable, R. M., H. I. Ingólfsson, …, R. W. Pastor. 2017. Lipid and peptide diffusion in bilayers: the Saffman-Delbrück model and periodic boundary conditions. *J. Phys. Chem. B.* 121:3443–3457.
44. Müller, T. J., and F. Müller-Plathe. 2009. Determining the local shear viscosity of a lipid bilayer system by reverse non-equilibrium molecular dynamics simulations. *Chemphyschem.* 10:2305–2315.
45. Lande, M. B., J. M. Donovan, and M. L. Zeidel. 1995. The relationship between membrane fluidity and permeabilities to water, solutes, ammonia, and protons. *J. Gen. Physiol.* 106:67–84.
46. Levental, I., D. Lingwood, …, K. Simons. 2010. Palmitoylation regulates raft affinity for the majority of integral raft proteins. *Proc. Natl. Acad. Sci. USA.* 107:22050–22054.
47. Corradi, V., B. I. Sejdiu, …, D. P. Tieleman. 2019. Emerging diversity in lipid-protein interactions. *Chem. Rev.* 119:5775–5848.
48. Machta, B. B., S. Papanikolaou, …, S. L. Veatch. 2011. Minimal model of plasma membrane heterogeneity requires coupling cortical actin to criticality. *Biophys. J.* 100:1668–1677.
49. Chichili, G. R., and W. Rodgers. 2007. Clustering of membrane raft proteins by the actin cytoskeleton. *J. Biol. Chem.* 282:36682–36691.
50. Dinic, J., P. Ashrafzadeh, and I. Parmryd. 2013. Actin filaments attachment at the plasma membrane in live cells cause the formation of ordered lipid domains. *Biochim. Biophys. Acta.* 1828:1102–1111.
51. Anderson, J. A., C. D. Lorenz, and A. Travesset. 2008. General purpose molecular dynamics simulations fully implemented on graphics processing units. *J. Comput. Phys.* 227:5342–5359.
52. Glaser, J., T. D. Nguyen, …, S. C. Glotzer. 2015. Strong scaling of general-purpose molecular dynamics simulations on GPUs. *Comput. Phys. Commun.* 192:97–107.
53. Girard, M., A. Ehlen, …, M. O. de la Cruz. 2019. Hoobas: a highly object-oriented builder for molecular dynamics. *Comput. Mater. Sci.* 167:25–33.
54. Marrink, S. J., H. J. Risselada, …, A. H. de Vries. 2007. The MARTINI force field: coarse grained model for biomolecular simulations. *J. Phys. Chem. B.* 111:7812–7824.
55. Stukowski, A. 2009. Visualization and analysis of atomistic simulation data with OVITO the Open Visualization Tool. *Model. Simul. Mater. Sci. Eng.* 18:015012.

Biophysical Journal, Volume *119*

Supplemental Information

Regulating Lipid Composition Rationalizes Acyl Tail Saturation Homeostasis in Ectotherms

Martin Girard and Tristan Bereau

Supplementary information: Regulating lipid composition rationalizes acyl-tail saturation homeostasis in ectotherms

Martin Girard*
Max Planck Institute for Polymer Research, Ackermannweg 10, Mainz 55128, Germany

Tristan Bereau
Max Planck Institute for Polymer Research, Ackermannweg 10, Mainz 55128, Germany and
Van 't Hoff Institute for Molecular Sciences and Informatics Institute,
University of Amsterdam, Amsterdam 1098 XH, The Netherlands

SIMULATION DETAILS

Simulations are run using HOOMD-blue 2.4.0 [1, 2] with a custom plugin for semi-grand canonical moves, velocity rescaling thermostat [3] and Nosé-Hoover-Langevin barostat [4, 5]. The thermostat employs a time constant of $\tau_T = 1$ ps while the barostat has a coupling constant of $\tau_P = 2$, a friction coefficient of $\gamma_P = 1$ ps^{-1} with an integration step size of 10 fs. The simulation box is a hexagonal prism and the tilt factors are not allowed to change. Trajectories record one frame every 10^4 timesteps (every 100 ps). Analysis are ran using custom C++ code and makes use of the GSD file format API available at `https://github.com/glotzerlab/gsd`. The first 10 μs of the trajectory is discarded.

Semi-grand canonical moves are performed using the algorithm described in [6]. Briefly, the neighbor cell list is made to comprise an even number of cells in all directions, and every 20 timesteps ($20\Delta t = 200$ fs) one cell every two in all dimensions is picked (1/8 of the cells overall are picked). In those cells, a particle is chosen at random. If the particle is swappable, an attempt to change its type is made based on the Monte-Carlo criteria $P = \min(1, \exp(-\beta(\Delta E - \Delta\mu)))$.

Initial configurations of the bilayer is generated using hoobas [7] and incorporates 32745 MARTINI water beads ($\sim$ 82 water molecules per lipid). The system first undergoes a relaxation process. This consists of slowly increasing the ϵ and σ values of the Lennard-Jones potential, up to their normal values, while running the system in microcanonical ensemble with a limit on displacement of 0.001 nm every timestep, with no coulombic potentials and no semi-grand canonical moves. The rest of the relaxation is described below:

Integration	Timesteps	Δt (fs)	Parameters
NVT, Langevin	3×10^4	10^{-2}	$\gamma_T = 1000$ ps^{-1}, $k_BT = 0$
NVT, Langevin	10^4	10^{-1}	$\gamma_T = 10$ amu ps^{-1}, $k_BT = 0$
NVT, Langevin	10^5	1	$\gamma_T = 5$ amu ps^{-1}
			Coulombic potential and semi-grand canonical moves turned on
NVT, Langevin	2×10^5	1	$\gamma_T = 5$ amu ps^{-1}
NPT	4×10^5	0.3	$\tau_T = 5$ ps, $\tau_P = 80$, $\gamma_P = 5$ ps^{-1}
NPT	3×10^5	3	$\tau_T = 5$ ps, $\tau_P = 80$, $\gamma_P = 5$ ps^{-1}
NPT	2×10^5	3	$\tau_T = 5$ ps, $\tau_P = 20$, $\gamma_P = 1$ ps^{-1}
NPT	2×10^5	10	$\tau_T = 1$ ps, $\tau_P = 2$, $\gamma_P = 1$ ps^{-1}
NPT + langevin thermostat	5×10^4	3	$\tau_T = 1$ ps, $\tau_P = 2$, $\gamma_P = 1$ ps^{-1}, $\gamma_T = 5$ amu ps^{-1}
NPT	$> 1.3 \times 10^9$	10	production, $\tau_T = 1$ ps, $\tau_P = 2$, $\gamma_P = 1$ ps^{-1}

MARTINI FORCE-FIELD

The force-field described in [8] is used with the following exceptions. All angle potentials centered on unsaturated beads have the following parameters: $\theta_0 = 120°$, $k_\theta = 45$ kJ/mol. For lipids with 0 or 1 unsaturations per acyl tail, this is not different from the original MARTINI force-field. For lipids with 2 unsaturations, the first angle along the tail was originally $\theta_0 = 100°$ and $k_\theta = 10$ kJ/mol. Furthermore, all beads centered on unsaturations are either C3 or

* martin.girard@mpip-mainz.mpg.de

C4. This is a requirement of the way we implement the semi-grand canonical Monte-Carlo moves on GPU. The first version of cholesterol molecules (without virtual sites) are used.

LIPIDS

Lipids used here are comprised of two acyl tails, each of which can be either of four fatty acids for a total of 16 lipid types. These represent the following fatty acids: stearic acid (C18:0), oleic acid (C18:1, ω-9, Δ-9), linoleic acid (C18:2, $\omega-6$, Δ-9,12) and cis-vaccenic acid (C18:1, $\omega-7$, Δ-11). There are no restriction on which position (sn-1 or sn-2) these are placed, unlike in cells. We also note that MARTINI does not differentiate between C16 and C18 tails due to its four-to-one mapping.

TERNARY MIXTURE

With C3 beads, above 16 - 18 % cholesterol, ternary DPPC / DOPC / Cholesterol mixture phase separates into DOPC-rich and DPPC-rich phases. This is an experimentally known phase separation and was reported in 25 µs long simulations using the MARTINI force-field at 290K [9] for a single composition (5:3:4). In [10], 10 µs long simulations did not show any phase separation for 7:7:6 composition at 295K. The typical phase separation time we observed for our phase separation is 10 - 12 µs, suggesting that the thermodynamic drive for separation is small. Both of these articles were published before the virtual-site MARTINI cholesterol model [11] and thus use the same cholesterol model as us. In contrast, in [12], none of the DPPC / DOPC / Cholesterol mixtures phase separated. Whether this is induced by changes to the cholesterol model in 2015 or subtle effects of the positional restraints used in [12] is unknown. Nevertheless, all our simulations above 18% cholesterol phase separate at 300K. Replacing the C3 beads by C4 beads results in very fast ($< 1\mu$s) demixing, at all cholesterol concentrations. This makes direct comparison of properties between our complex membranes and ternary mixtures impossible.

NEMATIC ORDER PARAMETER

To compute the nematic order parameter, the **Q**-tensor is constructed from every bond in lipid molecules:

$$Q_{ij} = N_b^{-1} \sum_b b_i b_j - 1/3\delta_{ij}$$

Where b_i is the ith component of the unit vector of the bond b and the lipids have N_b bonds overall. The eigenvalues of the tensor is computed using the Eigen package `http://eigen.tuxfamily.org/`. The largest eigenvalue defines the order parameter λ_+.

VISCOSITY

The viscosity is calculated through the orientational relaxation time. For every lipid molecule, we compute its q-tensor and obtain its director, $\vec{d}$, from the eigenvector corresponding to the largest eigenvalue. We then compute the orientational correlation function:

$$C(\Delta t) = \langle P_2(\vec{d}(t+\Delta t) \cdot \vec{d}(t)) \rangle$$

Where $P_2 = 3/2x^2 - 1/2$ is the second Legendre polynomial. Averaging is done over all molecules and we take one reference frame every 256 frames of the trajectory. The first 100 ns of the orientational correlation function is then fitted (with correlation coefficient $r^2 > 0.995$) to a stretched exponential function $C(t) = a\exp(-(t/t_0)^\beta) + (1-a)$ and the relaxation time is obtained by integrating the stretched exponential, $\tau = t_0\beta^{-1}\Gamma(\beta^{-1})$, which can be related to the viscosity (η) through $\tau = \eta\pi r^2 h/k_B T$, where h is half the bilayer height and $r = (A/\pi)^{1/2} \sim 0.4$ nm is the size of a lipid molecule, with A being the area per lipid.

As mentioned in the main text, values of viscosity on the order of 10^{-2} P have been measured in other simulations as well. This has been measured for MARTINI, CHARMM36 as well as GROMOS96 force-fields. Viscosity was

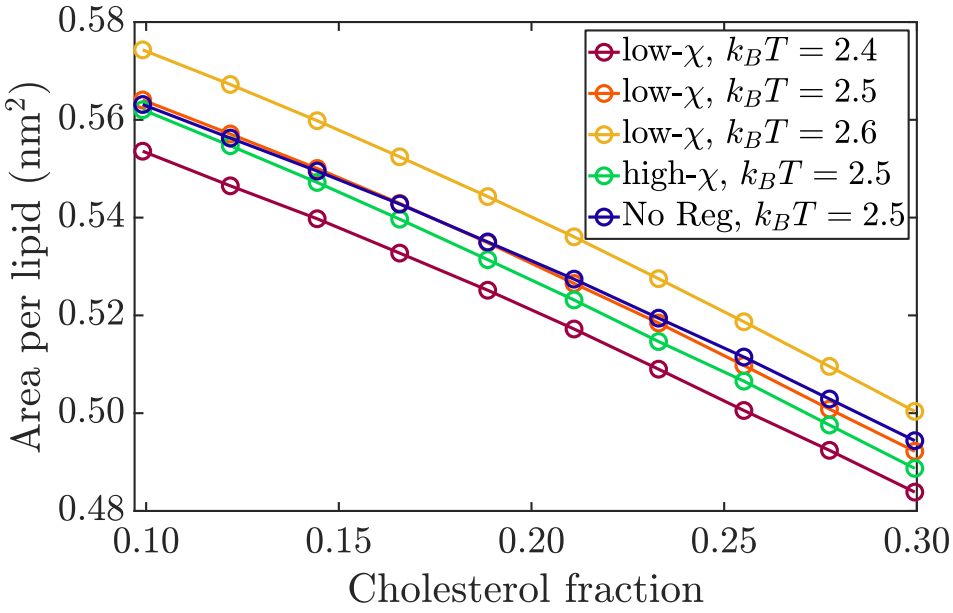

Figure S 1. Area available per lipid, computed from the size of each voronoi cell belonging to lipid molecules

calculated using periodic Saffman-Delbrück diffusion model (MARTINI and CHARMM36), reverse non-equilibrium molecular dynamics (GROMOS 96) and rotational diffusion correlation here. In [13], the value is compared favorably with a disordered n-hexadecane system ($\eta = 2.8 \times 10^{-2}$ P). It is possible that the lipid chosen here lead to a phase that is less ordered than biological membranes. For instance, in [14], by taking a lipid composition representative of plasma membrane at 310K ($k_{\mathrm{B}}T = 2.56$ kJ/mol) and 30% cholesterol, they find a nematic order parameter $\lambda_+ = 0.31 \sim 0.34$, which is slightly than in our simulations at similar parameters ($\lambda_+ = 0.30 \sim 0.31$). It is also possible that proteins, lipid rafts and other objects such as actin networks contribute to measured cell viscosities.

CORRELATION LENGTHS

The correlation length is obtained by computing a local value of λ_+ a 16×16 grid for each leaflet, and computing the spectral power $P(k) = |\mathcal{F}(\lambda_+(x, y))|^2$, where $\mathcal{F}$ is the Fourier transform. We use the fftw package (http://www.fftw.org/) to compute the Fourier transform through an FFT. The spectral power is then averaged through time, is then inverted and fitted to an exponential function: $\mathcal{F}^{-1}\left(\langle P(k)\rangle\right)(x, y) = \exp(-r/r_0)$, where $r = \sqrt{x^2 + y^2}$ and r_0 is the correlation length.

AREA PER LIPID

The area occupied by each lipid is computed by mapping lipids of each leaflet on a 2D plane, then using a voronoi tesselation to compute the area available to each lipid, shown in Fig. 1. We used the voronoi package from JCash, available at https://github.com/JCash/voronoi to perform the tesselation.

DIFFUSION

Diffusion constants are computed by measuring the mean squared displacement $R(\Delta t) = \langle (r(t + \Delta t) - r(t))^2 \rangle$, which at long times yields the lateral diffusion constant D through: $R(t) = 4Dt$, which is evaluated by fitting the curve $R(t)$. The averaging is done over all lipids and we take one reference frame every 256 frames of the trajectory. Diffusion constants are shown in Fig. 2.

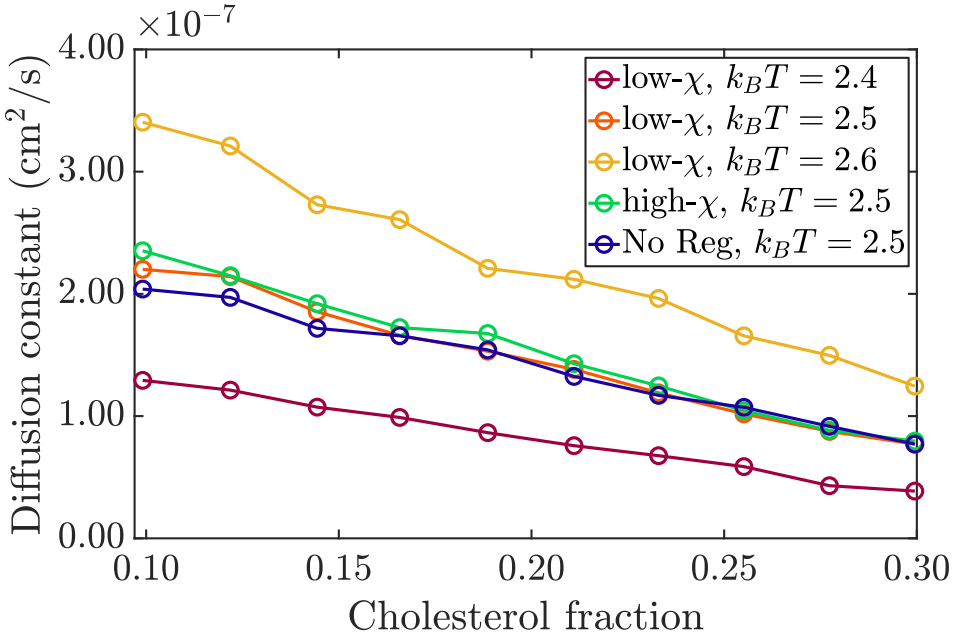

Figure S 2. Diffusion constants computed by fitting the mean-squared displacement $R(t) = 4Dt$

LIPID COMPOSITION AT DIFFERENT TEMPERATURES

The overall picture of acyl tail composition versus cholesterol fraction does not change much at different temperatures. However, the bilayers incorporate more unsaturated lipids to increase the mixing entropy. Curves are shown in Fig. 3 for both $k_\mathrm{B}T = 2.4$ and $k_\mathrm{B}T = 2.6$.

[1] J. A. Anderson, C. D. Lorenz, and A. Travesset, "General purpose molecular dynamics simulations fully implemented on graphics processing units," *Journal of Computational Physics*, vol. 227, pp. 5342–5359, May 2008.

[2] J. Glaser, T. D. Nguyen, J. A. Anderson, P. Lui, F. Spiga, J. A. Millan, D. C. Morse, and S. C. Glotzer, "Strong scaling of general-purpose molecular dynamics simulations on GPUs," *Computer Physics Communications*, vol. 192, pp. 97–107, July 2015.

[3] G. Bussi, D. Donadio, and M. Parrinello, "Canonical sampling through velocity rescaling," *The Journal of Chemical Physics*, vol. 126, p. 014101, Jan. 2007.

[4] G. J. Martyna, D. J. Tobias, and M. L. Klein, "Constant pressure molecular dynamics algorithms," *The Journal of Chemical Physics*, vol. 101, pp. 4177–4189, Sept. 1994.

[5] S. E. Feller, Y. Zhang, R. W. Pastor, and B. R. Brooks, "Constant pressure molecular dynamics simulation: The Langevin piston method," *The Journal of Chemical Physics*, vol. 103, pp. 4613–4621, Sept. 1995.

[6] B. Sadigh, P. Erhart, A. Stukowski, A. Caro, E. Martinez, and L. Zepeda-Ruiz, "Scalable parallel Monte Carlo algorithm for atomistic simulations of precipitation in alloys," *Physical Review B*, vol. 85, p. 184203, May 2012.

[7] M. Girard, A. Ehlen, A. Shakya, T. Bereau, and M. O. de la Cruz, "Hoobas: A highly object-oriented builder for molecular dynamics," *Computational Materials Science*, vol. 167, pp. 25–33, Sept. 2019.

[8] S. J. Marrink, H. J. Risselada, S. Yefimov, D. P. Tieleman, and A. H. de Vries, "The MARTINI Force Field: Coarse Grained Model for Biomolecular Simulations," *The Journal of Physical Chemistry B*, vol. 111, pp. 7812–7824, July 2007.

[9] S. Baoukina, E. Mendez-Villuendas, and D. P. Tieleman, "Molecular View of Phase Coexistence in Lipid Monolayers," *Journal of the American Chemical Society*, vol. 134, pp. 17543–17553, Oct. 2012.

[10] R. S. Davis, P. B. Sunil Kumar, M. M. Sperotto, and M. Laradji, "Predictions of Phase Separation in Three-Component Lipid Membranes by the MARTINI Force Field," *The Journal of Physical Chemistry B*, vol. 117, pp. 4072–4080, Apr. 2013.

[11] M. N. Melo, H. I. Ingólfsson, and S. J. Marrink, "Parameters for Martini sterols and hopanoids based on a virtual-site description," *The Journal of Chemical Physics*, vol. 143, p. 243152, Dec. 2015.

[12] T. S. Carpenter, C. A. López, C. Neale, C. Montour, H. I. Ingólfsson, F. Di Natale, F. C. Lightstone, and S. Gnanakaran, "Capturing Phase Behavior of Ternary Lipid Mixtures with a Refined Martini Coarse-Grained Force Field," *Journal of Chemical Theory and Computation*, vol. 14, pp. 6050–6062, Nov. 2018.

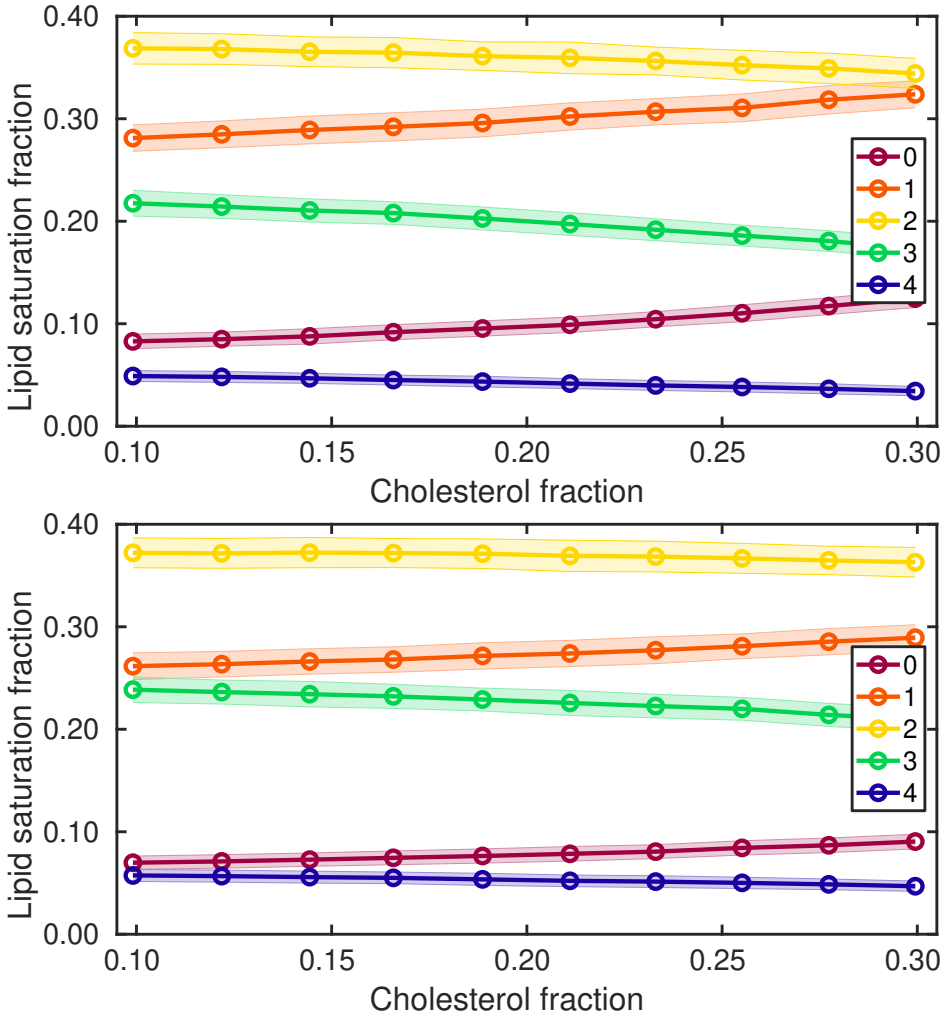

Figure S 3. Saturation contents of the low-χ (C3 Beads) lipid bilayer at different temperatures as a function of cholesterol, (top) $k_{\mathrm{B}}T = 2.4$, (bottom) $k_{\mathrm{B}}T = 2.6$

[13] T. J. Müller and F. Müller-Plathe, "Determining the Local Shear Viscosity of a Lipid Bilayer System by Reverse Non-Equilibrium Molecular Dynamics Simulations," *ChemPhysChem*, vol. 10, no. 13, pp. 2305–2315, 2009.

[14] H. I. Ingólfsson, M. N. Melo, F. J. van Eerden, C. Arnarez, C. A. Lopez, T. A. Wassenaar, X. Periole, A. H. de Vries, D. P. Tieleman, and S. J. Marrink, "Lipid Organization of the Plasma Membrane," *Journal of the American Chemical Society*, vol. 136, pp. 14554–14559, Oct. 2014.